doi: 10.56761/EFRE2022.C6-O-033604

Influence of helium ion irradiation on the stress evolution in nc-ZrN/a-ZrCu multilayered films

V.V. Uglov[1,], S.V. Zlotski[1], G. Abadias[2], I.S. Veremei*

[1]*Belarusian State University, Minsk, Belarus*
[2]*Institut Pprime, CNRS-Université de Poitiers- ENSMA, France*
[*]*uglov@bsu.by*

Abstract. The paper presents the results of stress evolution in nc-ZrN/a-ZrCu multilayered films with different Cu concentration (from 44.6 to 73.8 at.%) and thickness of amorphous layer ZrCu (5 and 10 nm) after He^{2+} (40 keV and fluences from 5.0×10^{16} to 1.1×10^{18} cm^{-2}) ion irradiation. It has been found that irradiation with helium ions leads to a decrease in the level of compressive stresses. In this case, for multilayer films with an amorphous layer thickness of 5 nm at a dose of more than 9.0×10^{18} cm^{-2}, the stresses decrease to zero and become tensile. The decrease in the stress level is mainly associated with the effects of radiation erosion of multilayer films.
Keywords: multilayered films, helium ion irradiation, stress, amorphous layers.

1. Introduction

Nowadays the development of new radiation-resistant materials is a crucial problem that is especially urgent for fission/fusion industry, aerospace application, etc. wherein objects are exposed to strong irradiation with ions, neutrons, electrons. So irradiation with light ions due to nuclear collisions can induce a higher ratio of point defects (e.g. vacancies and interstitials) produced relative to defect clusters (e.g. He bubbles) in metallic crystals [1]. This in turn remarkably degrades the performance of structural materials in advanced fission/fusion reactors, which must be significantly improved to extend the reliability and efficiency [2].

So it's necessary to create materials with a large number of sinks for point defects, such as dislocations, grain boundaries, and interphase boundaries to achieve this goal [3]. Nanostructured materials, such as nanocrystalline [4] and multilayer materials [5], contain abundant interfaces, which can serve as effective defect sinks to absorb irradiation-generated defects and relieve radiation damage [6]. Multilayer systems are promising for research because interlayer boundaries can affect the removal of radiation-induced defects. They have significant interphase regions, which can act as stable sinks of defects. Misra et al. [7] showed that Cu/Nb layer interfaces curtail the nucleation and growth of He bubbles. The ability of layer interfaces to trap defect clusters and reduce radiation damage has also been reported in other systems, such as Cu/V [8], Al/Nb [9], Cu/Mo [10], and Fe/W [11] and etc. Generally, the reduction in layer thickness leads to enhanced radiation performance due to the increasing density of layer interfaces.

One of the most promising materials with the large number of grain boundaries is nanocrystalline coatings, for example nc-ZrN, formed by vacuum arc deposition [12]. Deposited layers can exhibit a susceptibility to blistering that is dependent on the layer structure and composition, as well as on the presence of interfaces. Nanocrystalline coatings with crystalline/amorphous interfaces (such as nanocomposite ZrSiN and multilayered nc-MeN/a-Si_3N_4 systems) exhibit a high radiation tolerance along with crystalline/crystalline systems and decrease in radiation surface erosion, due to amorphous nanolayers associated with excellent defects absorption capability [13, 14]. Zhang et al. [15] showed size-dependent radiation tolerance of Cu/amorphous-CuZr nanolaminates against He implantation. Yu et al. [16] showed that irradiation-induced Fe/amorphous-FeZr interfaces could absorb defects and confine the movement of dislocation loops in crystalline layers to annihilate opposite defects under in situ Kr ion irradiation. However, questions such as irradiation-induced grain growth, phase stability of amorphous layers, and effects of crystalline/amorphous interfaces on radiation tolerance remain to be elucidated further.

2. Experimental details

nc-ZrN/a-ZrCu multilayer films were grown at 300 °C by magnetron sputter-deposition in a high-vacuum chamber (base pressure $<10^{-5}$ Pa) equipped with three confocal targets configuration and a cryogenic pump (max. 500 l/s). Films were deposited on Si (100) substrates covered with 10 nm thick thermally grown SiO_2 amorphous layer. A constant bias voltage of –60 V was applied to the substrate during deposition, while the substrate was rotated at 15 rpm throughout the whole deposition to ensure an equal deposition rate across the substrate area.

Water-cooled, 7.62-cm-diameter Zr (99.92% purity) and Cu (99.9% purity) targets, located at 18 cm from the substrate holder, were operated at constant power mode using a DC power supply and unbalanced magnetic configuration. A pure Ar discharge was used for the growth of $Zr_{1-x}Cu_x$ layers obtained by co-deposition, while a mixed Ar/N_2 plasma was employed to deposit ZrN layers by reactive sputtering. The total working pressure was 0.21 Pa, as measured using a Baratron® capacitance gauge. The Ar/N_2 flow ratio was optimized to obtain a Zr/N ratio close to 1.0 (stoichiometry) based on earlier results [17]. The N_2 partial pressure was measured and controlled during deposition using a MKS Microvision mass spectrometer.

nc-ZrN/a-$Zr_{1-x}Cu_x$ multilayer films with different Cu content x and thickness of ZrN and $Zr_{1-x}Cu_x$ elementary layers have been investigated. The Cu content in the $Zr_{1-x}Cu_x$ layers was varied by changing the DC power supply of the Cu target, from 40 to 52 W, and the DC power supply of Zr target, from 88 up to 294 W. As a result, $Zr_{1-x}Cu_x$ layers with x content ranging from 0.45 to 0.74 were synthesized, as determined from elemental probe microanalysis. The main characteristics of investigated nc-ZrN/a-$Zr_{1-x}Cu_x$ multilayer films are listed in Table 1.

Table 1. Characteristics of nc-ZrN/a-ZrCu multilayers: thickness ratio of ZrN and ZrCu elementary layers, total film thickness, range of He ions

Zr power (W)	Cu power (W)	Cu content in $Zr_{1-x}Cu_x$ layer	Total film thickness (nm)		Projected range R_p of He ions calculated by SRIM (nm)	
			ZrN(5 nm)/ ZrCu(5 nm)	ZrN(5 nm)/ ZrCu(10 nm)	ZrN(5 nm)/ ZrCu(5 nm)	ZrN(5 nm)/ ZrCu(10 nm)
294	40	0.45	298	302	153	159
243	52	0.53	296	300	153	158
164	51	0.61	299	301	152	156
88	51	0.74	292	296	152	154

The periodic growth of ZrN/ZrCu layered stack was monitored by computer-controlled pneumatic shutters located at 2 cm in front of each target. The deposition process always started with the ZrN sub-layer being deposited first. The total film thickness was about 300 nm (Table 1). Another film series, namely $Zr_{1-x}Cu_x$ monolithic films with the same Cu content and same total thickness, was also prepared for reference purpose.

Ion implantation of the nc-ZrN/a-$Zr_{1-x}Cu_x$ multilayered films was carried out using 40 keV He^{2+} ions at the DC-60 heavy-ion accelerator at the fluence from 5.0×10^{16} to 1.1×10^{18} cm^{-2}. Irradiation with helium ions was perpendicular to the surface of the samples. The implantation temperature was 300 K. The beam current was 20 μA, and water cooling of the target substrate was used. The energetic parameters of implantation were chosen so as the implanted He distribution depth did not exceed the film thickness, as calculated using the SRIM-2012 code [18].

X-ray Diffraction (XRD) analysis was employed for structural identification using an Ultima IV Rigaku X-ray diffractometer operating in parallel configuration and equipped with CuKα wavelength (0.15418 nm). XRD scans were collected at an incidence angle of 5°. The stresses in the films were determined by the $\sin^2\psi$ method for ZrN (200). The stresses were calculated using the elastic modulus and Poisson's ratio of 402 GPa and 0.26.

3. Structure and stress in nc-ZrN/a-ZrCu films

3.1. As-deposited films state

Fig.1 displays the XRD patterns of as-deposited monolithic $Zr_{1-x}Cu_x$ reference films with Cu content x = 0.45, 0.53, 0.61 and 0.74. For all films, the presence of a broad halo, characteristic of the first sharp diffraction peak in metallic glass films [19, 20], is observed. This indicates the formation of amorphous films in the investigated compositional range. The angular position of this peak changes from 37.15 to 41.35° with increasing Cu content from x = 0.45 to x = 0.74, suggesting a decreasing bonding length when Cu atoms substitute from Zr ones [21].

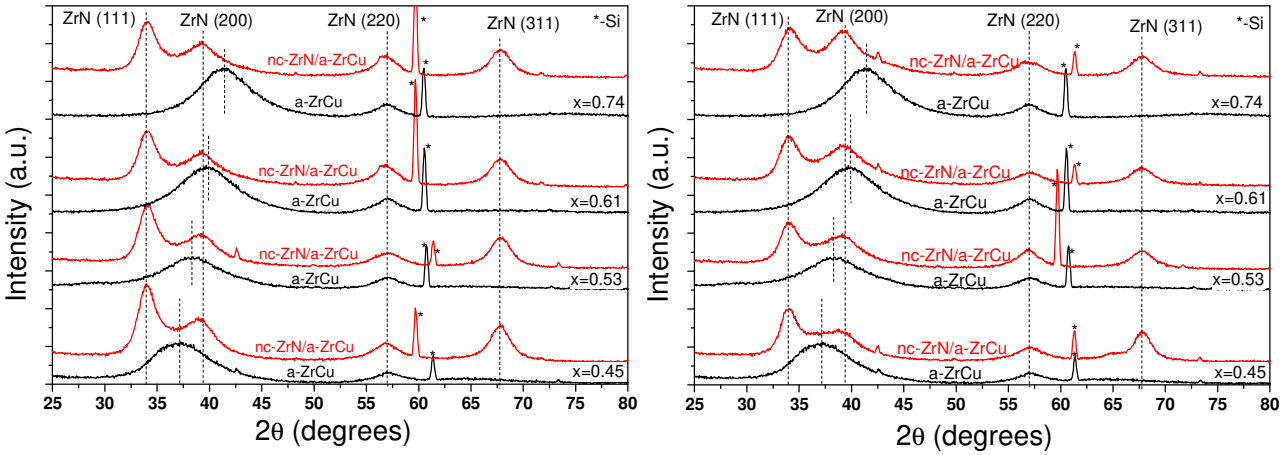

Fig.1. XRD patterns of as-deposited a-$Zr_{1-x}Cu_x$ amorphous, nc-ZrN/a-$Zr_{1-x}Cu_x$ (5 nm/5 nm) (a) and nc-ZrN/a-$Zr_{1-x}Cu_x$ (5 nm/10 nm) multilayered films with different cupper concentration x.

XRD patterns of as-deposited nc-ZrN/a-ZrCu (5 nm/5 nm) and nc-ZrN/a-ZrN (5 nm/10 nm) multilayered films are shown in Fig. 1. Diffraction lines corresponding to cubic (Na-Cl type) lattice of ZrN are clearly identified for both investigated bilayer periods. Bragg reflections from (111), (200), (220) and (311) planes are observed, attesting the formation of polycrystalline layers. The position of these lines remains practically unchanged when the metallic glass layer thickness changes from 5 to 10 nm. One can only note different intensity profile due to the convolution between a broad halo of the $Zr_{1-x}Cu_x$ layer and the diffraction lines from ZrN layer.

3.2. Irradiated films

Before investigating the surface of irradiated films, calculations using SRIM program were performed. For these calculations, the densities of ZrN and ZrCu layers, taken from the XRR investigations were used [21]. The results of SRIM calculations are presented in Table 1, where the projected range of the He distribution, R_p, is reported. The maximum He concentration is found to be located in the ZrN layers. SRIM calculations showed that the mean projected range R_p of He is 152–153 nm for nc-ZrN/a-$Zr_{1-x}Cu_x$ (5 nm/5 nm) and 154–159 nm for nc-ZrN/a-$Zr_{1-x}Cu_x$ (5 nm/10 nm), depending on Cu content, see Table 1.

The results of influence of He ions irradiation on the structure of nc-ZrN/a-$Zr_{1-x}Cu_x$ multilayer films are presented on the Fig.2. It was found that irradiation at the fluence up to 1.1×10^{18} cm^{-2} did not change the phases composition of films. We see a small shift the position of the ZrN diffraction peaks (change in lattice parameter) for low fluences and big shift for high fluences (Fig.2). It has been found that the largest changes in the lattice parameter are observed for films with a smaller thickness of the amorphous layer ZrCu.

It is also seen that irradiation with helium ions leads to a decrease in the intensity of the ZrN (111) diffraction peak and an increase in the intensity of the (200) peak. A decrease in the intensity and width of diffraction peaks was revealed, which is associated with surface erosion [21] and stress relaxation. It was found that the ZrN phase is retained at a maximum fluence of 1.1×10^{18} cm^{-2} (Fig.2).

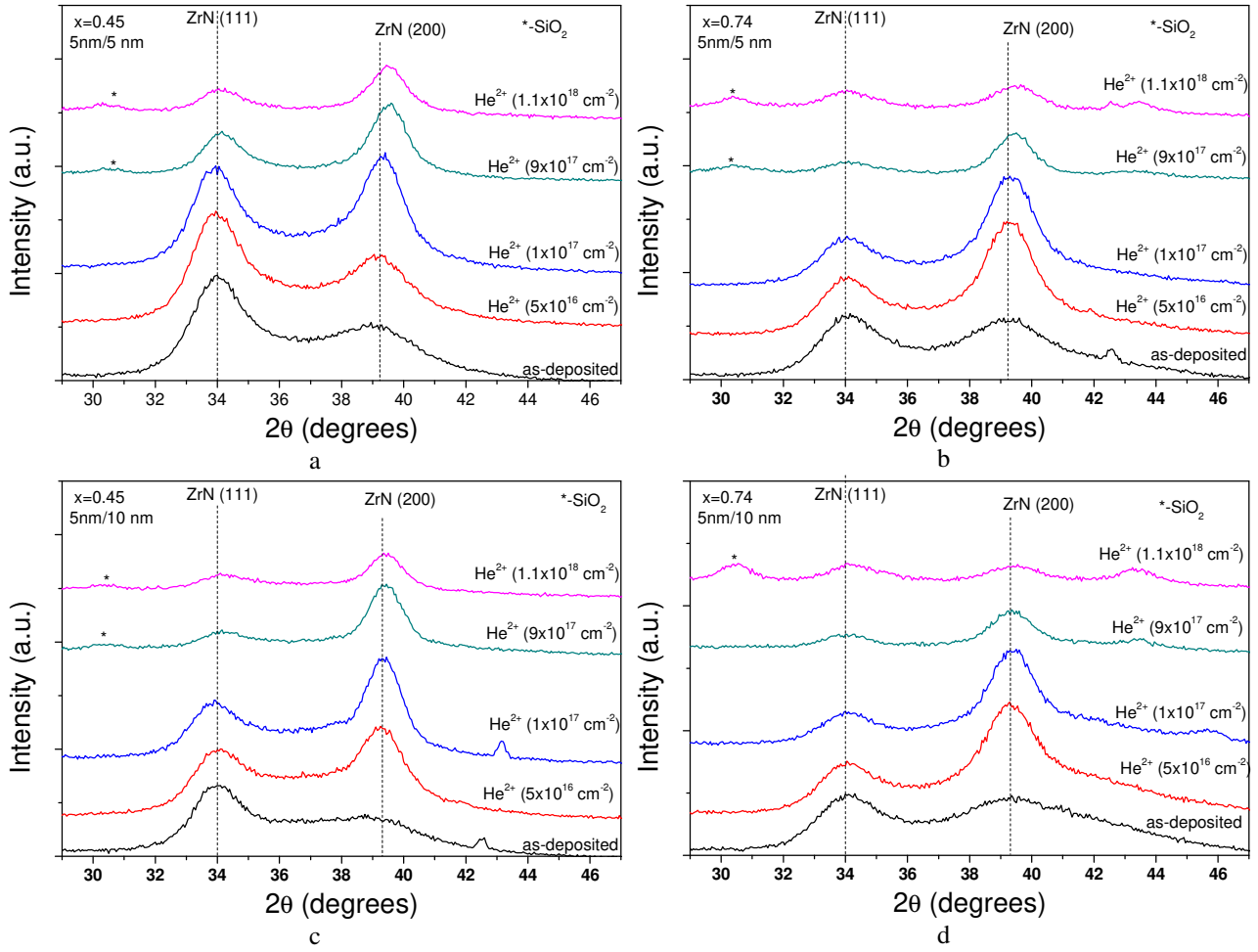

Fig.2. XRD patterns of nc-ZrN/a-$Zr_{1-x}Cu_x$ (5 nm/5 nm) (a, b) and nc-ZrN/a-$Zr_{1-x}Cu_x$ (5 nm/10 nm) (c, d) multilayered films with x=0.45 (a, c) and x=0.74 (b, d) irradiated with 40 keV He^{2+} ions at different fluences.

The detected shift of the ZrN diffraction peaks is related to the behavior of stresses in the films upon irradiation with helium ions. The results of stress calculations using the $\sin^2\psi$ method are shown in Fig.3.

As can be seen from Fig.3 initial films have compressive stresses. For the thickness of the amorphous layer, the stress level is about –1.5 GPa, and for 10 nm it decreases with increasing copper concentration in the amorphous layer. It was found that irradiation with helium ions with a fluence of 5×10^{16} cm^{-2} leads to an increase in the stress level. In this case, the greatest change in the stress level is observed for the copper content of 0.45 and 0.74. A further increase in fluence leads to a decrease in compressive stresses (Fig.3). A gradual decrease in the level of compressive stresses with increasing fluence is observed. It should be noted that for an amorphous layer thickness of 5 nm, the final stress level is lower than for a thickness of 10 nm (Fig.3). In this case, for an amorphous layer thickness of 5 nm and a low copper content in the ZrCu layer at high fluences, the stresses become tensile.

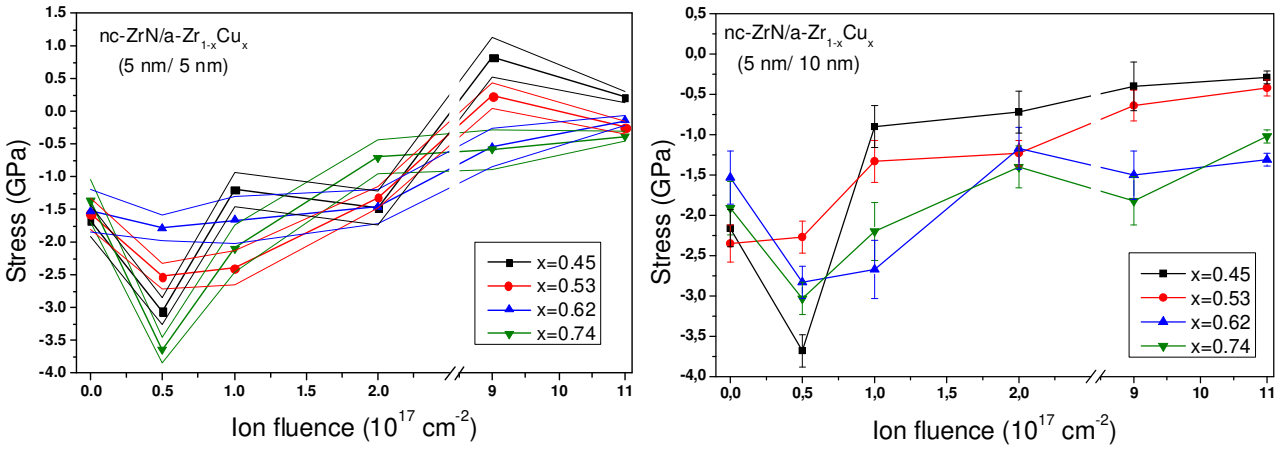

Fig.3. Dependence of stresses in nc-ZrN/a-$Zr_{1-x}Cu_x$ (5 nm/5 nm) (a) and nc-ZrN/a-$Zr_{1-x}Cu_x$ (5 nm/10 nm) (b) multilayered films on fluence of He^{2+} ions.

This behavior of stresses in films during irradiation can be explained by the formation of radiation defects during irradiation with helium ions. At low doses, radiation defects (interstitial atoms and vacancies) and helium-vacancy clusters are formed in ZrN, which leads to a significant increase in the level of compressive stresses. Further irradiation results in the formation of nanosized helium bubbles and stress relaxation. Further irradiation promotes the migration of radiation defects and helium-vacancy clusters into amorphous layers, which leads to a decrease in the level of compressive stresses.

The decrease in the level of compressive stresses at high fluences is associated with the processes of radiation erosion of the surface of multilayer films. In this case, an increase in the copper content in the amorphous layer and the thickness of this layer up to 10 nm lead to an increase in the critical fluence, at which the film is eroded [21]. The latter, in turn, causes a high level of compressive stresses in these films compared to films with a low concentration of copper in the amorphous layer and a thickness of this layer of 5 nm.

4. Conclusion

nc-ZrN/a-$Zr_{1-x}Cu_x$ multilayered films with different thickness of elementary layers and Cu content in $Zr_{1-x}Cu_x$ layers were deposited by magnetron sputtering. The films consist of alternating crystalline ZrN and amorphous $Zr_{1-x}Cu_x$ layers. Multilayer films have compressive stresses, the level of which decreases with the copper content x in the a-$Zr_{1-x}Cu_x$ layer and increases with the thickness of this layer.

The stability of the phase composition of nc-ZrN/a-$Zr_{1-x}Cu_x$ multilayer films to irradiation with helium ions up to fluence of 1.1×10^{18} cm^{-2} has been established.

It was revealed that irradiation with helium ions leads to an increase in the level of compressive stresses, and then to a gradual decrease with increasing ion fluence. It has been established that an increase in the copper content x in the a-$Zr_{1-x}Cu_x$ layer and the thickness of this layer lead to a smaller decrease in the level of compressive stresses.

5. References

[1] Demkowicz M.J., Bhattacharyya D., Usov I., Wang Y.Q., Nastasi M., Misra A., *Appl. Phys. Lett.,* **97**, 161903, 2010; doi: 10.1063/1.3502594

[2] Jiao Z., Was G.S., *J. Nucl. Mater.,* **407**, 34, 2010; doi: 10.1016/j.jnucmat.2010.07.006

[3] Zhang Xinghang, et al., *Prog.Mat. Sc.,* **96**, 217, 2018; doi: 10.1016/j.pmatsci.2018.03.002

[4] El-Atwani O., Hattar K., Hinks J., Greaves G., Harilal S.S., Hassanein A., *J. Nucl. Mater.,* **458**, 216, 2015; doi: 10.1016/j.jnucmat.2014.12.095
[5] Chen Di, Li Nan, Yuryev Dina, Baldwin J. Kevin, Wang Yongqiang, Demkowicz Michael J., *Sci. Adv.,* **3** (11), eaao2710, 2017; doi: 10.1126/sciadv.aao2710
[6] Zhang Xinghang, Hattar Khalid, Chen Youxing, Shao Lin, Li Jin, Sun Cheng, Yu Kaiyuan, Li Nan, Taheri Mitra L., Wang Haiyan, Wang Jian, Nastasi Michael, *Prog. Mater. Sci.,* **96**, 217, 2018; doi: 10.1016/j.pmatsci.2018.03.002
[7] Misra A., Demkowicz M., Zhang X. and Hoagland R.G., *JOM,* **59**, 62, 2007; doi: 10.1007/s11837-007-0120-6
[8] Fu E.G., Misra A., Wang H., Shao Lin, Zhang X., *J. Nucl. Mater.,* **407**, 178, 2010; doi: 10.1016/j.jnucmat.2010.10.011
[9] Li N., Martin M.S., Anderoglu O., Misra A., Shao L., Wang H. and Zhang X., *J. Appl. Phys.,* **105**, 123522, 2009; doi: 10.1063/1.3138804
[10] Li N., Carter J.J., Misra A., Shao L., Wang H. & Zhang X., *Philos. Mag. Lett.,* **91**, 18, 2011; doi: 10.1080/09500839.2010.522210
[11] Li N., Fu E.G., Wang H., Carter J.J., Shao L., Maloy S.A., Misra A., Zhang X., *J. Nucl. Mater.,* **389**, 233, 2009; doi: 10.1016/j.jnucmat.2009.02.007
[12] Janse van Vuuren A., Sohatsky A., Uglov V., Skuratov V., Volkov A., *Phys. Status Solidi C,* **13**, 886, 2016; doi: 10.1002/pssc.201600027
[13] Uglov V.V., Abadias G., Zlotski S.V., Saladukhin I.A., Cherenda N.N., *Surf. Coat. Techn.,* **394**, 125654, 2020; doi: 10.1016/j.surfcoat.2020.125654
[14] Uglov V.V., et al., *Surf. Coat. Technol.,* **399**, 126146, 2020; doi: 10.1016/j.surfcoat.2020.126146
[15] Zhang J., Wang Y., Liang X., Zeng F.L., Liu G., Sunet J., *Acta Mater.,* **92**, 140, 2015; doi: 10.1016/j.actamat.2015.03.055
[16] Yu K.Y., Fan Z., Chen Y., Song M., Liu Y., Wang H., Kirk M.A., Li M.& Zhang X., *Mater. Res. Lett.,* **3**, 35, 2014; doi: 10.1080/21663831.2014.951494
[17] Abadias G., Uglov V.V., Saladukhin I.A., Zlotski S.V., Tolmachova G., Dub S.N., Janse van Vuuren A., *Surf. Coat. Technol.,* **308**, 158, 2016; doi: 10.1016/j.surfcoat.2016.06.099
[18] SRIM software. *The Stopping and Range of Ions in Matter* [online]; http://www.srim.org
[19] Apreutesei M., Djemia P., Belliard L., Abadias G., Esnouf C., Billard A., Steyer P., *J. Alloy. Comp.,* **707**, 126, 2017; doi: 10.1016/j.jallcom.2016.12.208
[20] Ghidelli M., et al., *Acta Mater.,* **213**, 116955, 2021; doi: 10.1016/j.actamat.2021.116955
[21] Uglov V.V., Abadias G., Zlotski S.V., Saladukhin I.A., Veremei I.S., *Surf. Coat. Technol.*, 128547, 2022; doi: 10.1016/j.surfcoat.2022.128547